Molecular Cell
Article

S6K1-Mediated Disassembly of Mitochondrial URI/PP1γ Complexes Activates a Negative Feedback Program that Counters S6K1 Survival Signaling

Nabil Djouder,[2,4] Stefan Christian Metzler,[2,5] Alexander Schmidt,[3,4,5] Christiane Wirbelauer,[1,5] Matthias Gstaiger,[2,4,6] Ruedi Aebersold,[3,4] Daniel Hess,[1] and Wilhelm Krek[2,4,*]
[1]Friedrich Miescher Institute for Biomedical Research, 4022 Basel, Switzerland
[2]Institute of Cell Biology
[3]Institute of Molecular Systems Biology
[4]Competence Center for Systems Physiology and Metabolic Diseases
Swiss Federal Institute of Technology (ETH) Zurich, 8093 Zurich, Switzerland
[5]These authors contributed equally to this work.
[6]Present address: Institute of Molecular Systems Biology, Swiss Federal Institute of Technology (ETH) Zurich, 8093 Zurich, Switzerland.
*Correspondence: wilhelm.krek@cell.biol.ethz.ch
DOI 10.1016/j.molcel.2007.08.010

SUMMARY

S6 kinase 1 (S6K1) acts to integrate nutrient and growth factor signals to promote cell growth but also cell survival as a mitochondria-tethered protein kinase that phosphorylates and inactivates the proapoptotic molecule BAD. Here we report that the prefoldin chaperone URI represents a mitochondrial substrate of S6K1. In growth factor-deprived or rapamycin-treated cells, URI forms stable complexes with protein phosphatase (PP)1γ at mitochondria, thereby inhibiting the activity of the bound enzyme. Growth factor stimulation induces disassembly of URI/PP1γ complexes through S6K1-mediated phosphorylation of URI at serine 371. This activates a PP1γ-dependent negative feedback program that decreases S6K1 activity and BAD phosphorylation, thereby altering the threshold for apoptosis. These findings establish URI and PP1γ as integral components of an S6K1-regulated mitochondrial pathway dedicated, in part, to oppose sustained S6K1 survival signaling and to ensure that the mitochondrial threshold for apoptosis is set in accord with nutrient and growth factor availability.

INTRODUCTION

Tissue homeostasis in multicellular organisms is controlled by the availability of growth factors that provide signals for the growth and proliferation of the constituent cells. When growth factors become limiting, cells cease growing and undergo apoptosis via an intrinsic cell death pathway initiated by mitochondria (Hammerman et al., 2004). Growth factor signaling also regulates cellular metabolism and allows for exogenous nutrient utilization (Plas and Thompson, 2005). The integration of growth factor and nutrient signals is achieved through mammalian target of rapamycin (mTOR), which coordinately controls cell growth by modulating the activity of a series of effector proteins. Among these is S6 kinase 1 (S6K1), which promotes protein synthesis as well as cell survival (Sabatini, 2006; Wullschleger et al., 2006).

The survival function of S6K1 is mediated, at least in part, as a mitochondria-bound enzyme that phosphorylates the death agonist BAD at Ser-136 in response to insulin-like growth factor (IGF)1 treatment (Harada et al., 2001). Also, other kinases phosphorylate and inactivate BAD, and depending on cellular context, include PKA for Ser-112 and Ser-155 sites, Akt/PKB for Ser-136, and RSK and MAPK for Ser-112 (Bergmann, 2002; Klumpp and Krieglstein, 2002). Phosphorylation of BAD at any of these three sites results in its association with 14-3-3 protein in the cytosol, thereby freeing BCL-2 and BCL-X_L to promote survival (Datta et al., 2000, 2002; Harada et al., 2001). Kinase-mediated inactivation of BAD is counterbalanced by phosphatases, including mitochondria-based BAD-bound phosphatase 1 (PP1) (Danial et al., 2003), suggesting that dynamic changes in the phosphorylation state of BAD mediated by opposing kinase-phosphatase activities serve as a critical mechanism by which cells set a mitochondrial threshold for apoptosis in response to survival signals and death cues.

Recently, we described the identification of *u*nconventional prefoldin *R*PB5 *i*nteractor (URI) (Gstaiger et al., 2003), an unconventional member of the prefoldin (PFD) family of chaperones. Conventional members of the PFD family are of small molecular weight (14–23 kDa) and are composed of N- and C-terminal α-helical coiled-coil structures connected by either one (β class PFD) or two (α class PFD) β hairpins (Siegert et al., 2000). Yeast and human

PFDs 1–6 assemble into an α2β4 hexameric complex, termed prefoldin/GimC (Martin-Benito et al., 2002; Siegers et al., 1999; Vainberg et al., 1998). URI's primary structure contains all features of an α class PFD but in addition contains an RPB5-binding segment and a long acidic C-terminal region. URI has been identified as part of a prefoldin/GimC-like complex containing the α class PFD STAP1 (Skp2-associated α class PFD) and the two β class PFDs PFD2 and PFD4-related (PFD4r), and non-PFD subunits including RPB5, TIP48, and TIP49 (Gstaiger et al., 2003). Functional analysis of URI in yeast revealed that it acts downstream of TOR to control nutrient-sensitive gene expression. In mammalian cells, the phosphorylation state of URI is influenced by signals that affect mTOR activity insofar as insulin or IGF1 treatment produces hyperphosphorylated URI, an effect blocked by rapamycin (Gstaiger et al., 2003). The tight correlation between URI phosphorylation and mTOR activity implies a potential role for URI in mTOR signaling in mammalian cells.

Here we report that URI associates with PP1γ at mitochondria and that stimulation of cells with IGF1 triggers S6K1-dependent phosphorylation of URI at Ser-371 and the dissociation of URI/PP1γ complexes. Released PP1γ contributes, in turn, to the downregulation of S6K1 activity in vivo, thereby diminishing BAD phosphorylation and enhancing a cell's susceptibility to undergo apoptosis. Our data identify URI as a mitochondrial substrate of S6K1 and suggest that S6K1-mediated phosphorylation of URI on Ser-371 in response to growth factors activates a mitochondria-based negative feedback mechanism that helps to restrict S6K1 pathway activity and thus ensures that cell death responses are coordinated with growth factor and nutrient signaling.

RESULTS

URI Is a Mitochondrial Protein and Is Phosphorylated in an S6K1-Dependent Manner

To gain insight into the regulation and function of URI, we assessed the intracellular localization of URI in human cells using affinity-purified URI polyclonal antibody anti-URI(Ct) and URI monoclonal antibodies (mAbs) 58.2 that recognize endogenous URI (see Figures S1A and S1B, respectively, in the Supplemental Data available with this article online). Immunostaining of HeLa cells with anti-URI(Ct) resulted in a predominantly punctate cytoplasmic signal (Figure 1A), which was blocked by preincubation with the GST-URI fusion protein against which anti-URI(Ct) was raised, but not by preincubation with GST alone (Figures 1C and 1B, respectively). Interestingly, two-color confocal microscopy with anti-URI(Ct) and the mitochondrial marker MitoTracker revealed a striking colocalization (Figures 1D–1F). Immunostaining with URI mAb 58.2 produced similar results in these cells (Figure 1K) and in multiple other human cell lines (data not shown). Thus, URI localizes to mitochondria.

Biochemical fractionation of HeLa cells revealed URI in nuclear, cytoplasmic, and mitochondrial fractions (Figure 1M). At mitochondria, URI is a component of the outer membrane fraction as evidenced by its Proteinase K sensitivity (Figure 1N). Unlike the cytoplasmic or nuclear pool of URI, the majority of mitochondrial URI migrated as a slower form (Figure 1M, compare lanes 1 and 2 with lane 3). As reported, the slower migrating band of URI is sensitive to phosphatase treatment, suggesting that it represents one or more hyperphosphorylated forms of URI (Gstaiger et al., 2003). Treatment of cells with rapamycin prior to cell fractionation converted the slower migrating, hyperphosphorylated form of URI into a faster migrating, un(der)phosphorylated species of URI (Figure 1O, lane 2). A similar effect was seen after knockdown of S6K1 by siRNAs (Figure 1O, lane 4). Also, the small fraction of cytoplasmic URI that migrated as a slower form was reduced following knockdown of S6K1 (Figure 1O, lane 6). Overexpression of a rapamycin-resistant allele of S6K1, myc-tagged S6K1(RR) (Pullen et al., 1998), promoted hyperphosphorylation of URI in the presence of rapamycin (Figure 1P, lane 5). Myc-S6K1(WT) was inactive in this regard (Figure 1P, lane 6). Finally, treatment of serum-starved cells with IGF1 induced hyperphosphorylation of URI (Figure 1Q, lane 6), which was efficiently blocked by either knockdown of S6K1 (lane 9) or by rapamycin (lane 10). These results suggest a tight correlation between S6K1 signaling and the appearance of slower migrating, hyperphosphorylated form(s) of URI at mitochondria.

S6K1 Phosphorylates URI In Vitro and In Vivo at Ser-371

The above results raise the possibility that URI represents a potential substrate of S6K1. Indeed, GST-URI full-length fusion protein was potently phosphorylated in vitro by myc-tagged S6K1(WT), but not kinase-inactive S6K1(KD) mutant protein (Figure 2A, lanes 2 and 3, respectively). Inspection of human URI primary sequence revealed two potential consensus phosphorylation sites for S6K located at amino acid residues 349 and 371 (Figure 2B). Indeed, a URI fragment corresponding to residues 357–420 was still potently phosphorylated by histidine (His_6)-tagged S6K1 (Figure S2, lane 8), while a URI segment spanning residues 418–534 was not (Figure S2, lane 10). These results suggest that Ser-371 of URI may represent a site for phosphorylation by S6K1 in vitro.

High-performance mass spectrometric (MS) analysis of trypsinized URI using two consecutive stages of fragmentation unambiguously identified Ser-371 to be phosphorylated by S6K1 in vitro (Figure S3). Label-free quantitative MS analysis revealed that Ser-371 of URI was specifically phosphorylated by S6K1 and that this site was much less phosphorylated, if at all, when ATP was omitted from the kinase reaction (Figure 2C). The degree of Ser-371 phosphorylation by S6K1 in vitro could be determined to be very high (75%), based on a 3-fold downregulation of non-phosphorylated Ser-371 after kinase reaction (Figure 2C). Whether URI is also phosphorylated in vitro on Thr-349

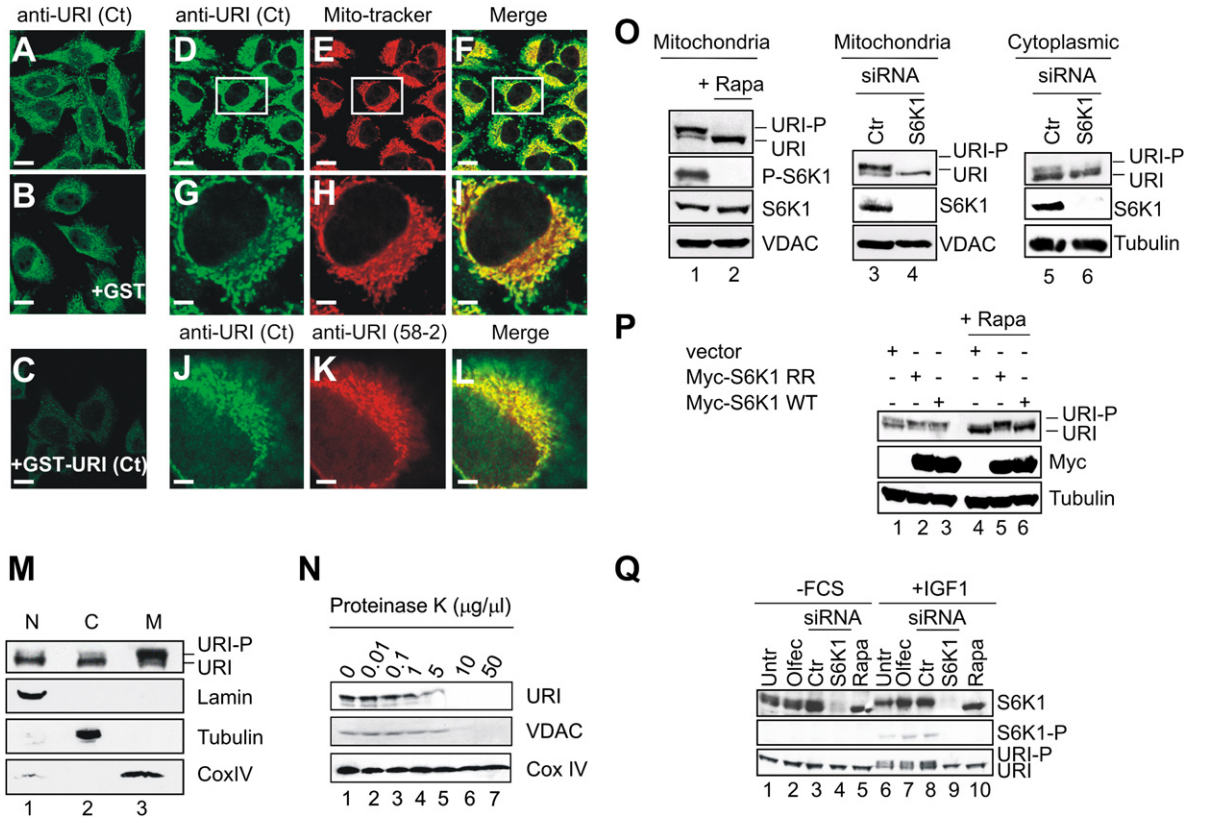

Figure 1. URI Is a Mitochondrial Protein and Substrate of S6K1

(A–C) HeLa cells were stained with anti-URI(Ct) antibody in the presence of GST (B) or GST-URI (418–534) fusion protein (C).

(D–I) HeLa cells were double stained with anti-URI(Ct) antibody (D) and MitoTracker (E). Merged URI and MitoTracker staining is shown (F). Enlargements of regions indicated by white rectangles (D–F) are shown in (G)–(I).

(J–L) HeLa cells were double stained with anti-URI(Ct) polyclonal (D) and anti-URI 58-2(K) monoclonal antibody. Merged URI stainings (L). For pictures A–F, scale bars represent 15 μm. For pictures G–L, scale bars represent 4 μm.

(M) Immunoblot of URI and phospho-URI (URI-P) levels in nuclear (lane 1), cytoplasmic (lane 2),and mitochondrial (lane 3) fractions.

(N) Mitochondrial fractions of HeLa cells treated with increasing amounts of Proteinase K were processed for immunoblotting.

(O) Immunoblots of URI, phospho-T389 S6K1, total S6K1, and VDAC of mitochondrial fractions from HeLa cells that were either untreated (lane 1), treated with 50 nM rapamycin (lane 2), or transfected with siRNA corresponding to a nonrelevant mRNA (lane 3) or *S6K1* mRNA (lane 4). Immunoblot of URI, S6K1, and tubulin of cytoplasmic fractions from HeLa cells transfected with siRNA corresponding to a nonrelevant mRNA (lane 5) or *S6K1* mRNA (lane 6).

(P) HEK293 cells were either transfected with a control plasmid (lanes 1 and 4), Myc-S6K1 rapamycin-resistant (RR) mutant (lanes 2 and 5), or Myc-S6K1(WT) (lanes 3 and 6) or treated with 50 nM of rapamycin (lanes 4–6), immunoprecipitated with 9E10 anti-myc mAb, and blotted for URI, Myc, and tubulin.

(Q) HeLa cells were either not transfected (lanes 1 and 6), treated with transfection reagent (lanes 2 and 7), transfected with control siRNA (lanes 3 and 8), transfected with S6K1(1)-siRNA (lanes 4 and 9), or treated with rapamycin (lanes 5 and 10). They were then either serum starved (lanes 1–5) or serum starved and stimulated with IGF1 (lanes 6–10) and analyzed by immunoblotting for total or pThr-389 S6K1 and URI.

could not be determined, because enzymatic cleavage of URI, even with different proteases, did not result in a peptide suitable for MS analysis.

To test whether URI is also phosphorylated in vivo at Ser-371, endogenous URI immunoprecipitates derived from HeLa cells were subjected to phosphorylation site analysis by targeted quantitative MS. We detected very little, if any, pSer-371 in URI immunoprecipitates from serum-deprived HeLa cells (Figure 2D). Treatment of cells with IGF1 dramatically increased Ser-371 phosphorylation of URI, while rapamycin blocked phosphorylation on that site (Figure 2D). Similar results were obtained in HEK293 and U2OS cells (Figures S4A and S4B, respectively). Thus, URI is phosphorylated in vivo at Ser-371 in a growth factor- and rapamycin-dependent manner, supporting the view that URI represents a potential substrate of S6K1.

URI Associates with PP1γ in a Growth Factor-Dependent Manner

To uncover potential consequences of S6K1-mediated phosphorylation of URI at Ser-371, we sought next for proteins that might bind to URI in a phosphorylation-dependent manner. To this end, we performed MS

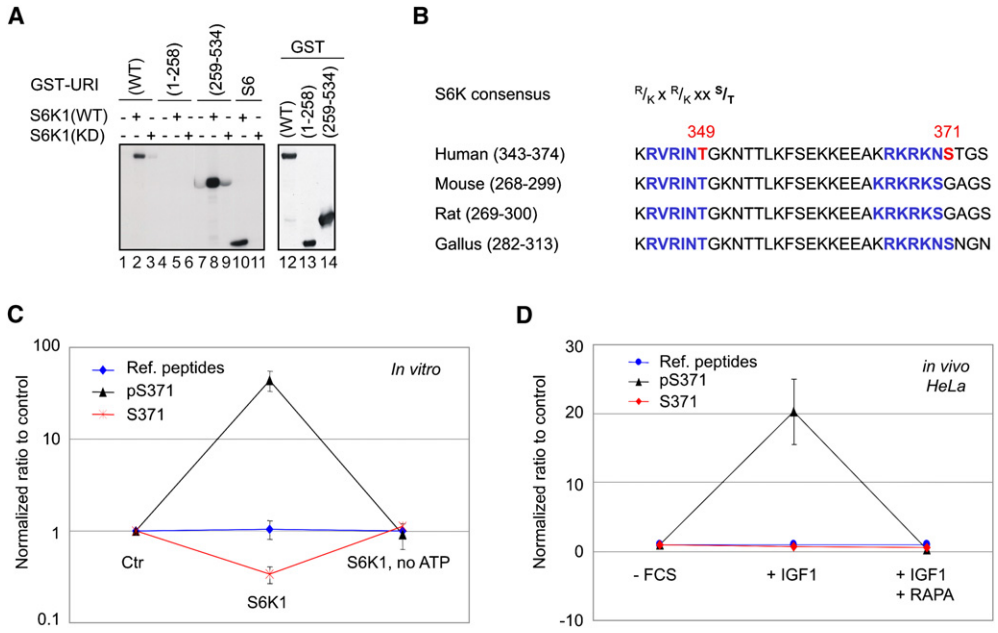

Figure 2. S6K1 Phosphorylates URI In Vitro and In Vivo on Ser-371

(A) Myc-S6K1(WT) or kinase-dead (KD) mutant was transfected, immunoprecipitated with 9E10 anti-myc mAb, and used for in vitro kinase assays with baculovirus-produced and λ-phosphatase-treated, purified GST-URI(WT), or indicated fragments of it as substrate (lanes 1–9). 40S ribosomal protein S6 served as control (lanes 10 and 11). Amounts of different GST-URI fusion proteins were used for in vitro kinase reactions as measured by immunoblotting with anti-GST antibody (lanes 12–14).

(B) Alignment of amino acid sequences of URI from different species encompassing the S6K consensus phosphorylation site motifs.

(C and D) Quantitative LC-MS/MS analysis of pSer-371 in vitro and in vivo. Averaged and normalized abundance profiles of the tryptic URI peptide "KN*p*STGSGHSAQELPTIR" phosphorylated at Ser- 371 (pS371, black), its nonphosphorylated counterpart (S371, red), and five unmodified reference peptides of URI (reference, blue) are shown. Ratio deviations between LC-MS analyses of multiple samples are indicated in error bars. (C) Intensity profiles obtained from an in vitro assay of control (URI expressed in *E. coli*), S6K1 (URI incubated with S6K1 in the presence of ATP), and S6K1 no ATP (URI incubated with S6K1 without ATP). (D) pSer-371 abundance profile of endogenous URI immunoprecipitates derived from HeLa cells that had been either serum starved (−FCS), serum starved and restimulated with IGF1 (−FCS + IGF1), or serum starved and rapamycin treated and restimulated with IGF1 (−FCS + IGF1 + RAPA) is shown.

identification of URI-associated proteins from serum-starved HEK293 cells. Among the proteins specifically enriched in URI (but not control) immunoprecipitates was PP1γ (Figure 3A, lane 2). We also detected URI in endogenous PP1γ immunoprecipitates from HeLa whole-cell extracts (Figure 3B, lane 3). Notably, PP1γ immunoprecipitates were selectively enriched for the un(der)phosphorylated form of URI (Figure 3B, lane 3), implying that URI/PP1γ interactions may be dynamically regulated by phosphorylation (see below). PP1γ interacted also with URI when both were coexpressed as epitope-tagged species in HEK293 cells (Figure S5A) and bound to each other in GST pull-down assays (Figures S5B and S5C). Biochemical cell fractionation revealed that PP1γ is also present at mitochondria (Figure 3C, lane 3), as are other PFD subunits that are known to interact with URI, including STAP1, PFD2, and PFD4r (Figure 3C, lane 3).

Importantly, association of URI with PP1γ in vivo is regulated by growth factors. PP1γ immunoprecipitates from serum-starved HeLa cells contained abundant URI (Figure 3D, lane 3). IGF1 stimulation caused a drastic reduction in PP1γ-associated URI (Figure 3D, lanes 6 and 9, respectively). This was accompanied by hyperphosphorylation of URI (Figure 3D, lanes 14 and 15). Addition of rapamycin to IGF1-stimulated cells reversed this effect (Figure 3D, lane 12). This coincided with un(der)-phosphorylation of URI (Figure 3D, lane 16). URI/PP1γ complexes dissolve as early as 15–30 min after IGF1 treatment (Figure S6A). Similar results were obtained in U2OS cells (Figure S6B). Rapamycin also enhanced URI/PP1γ complex formation at mitochondria (Figure S7A, compare lanes 6 and 3) and, as expected, promoted the interaction of URI-associated PFD subunits STAP1, PFD2, and PFD4r with PP1γ in vivo at mitochondria (Figure S7B). These results suggest that PP1γ associates with the un(der)-phosphorylated form of URI in vivo and that growth factor signaling promotes dissociation of URI/PP1γ complexes.

Phosphorylation of URI at Ser-371 by S6K1 Relieves URI-Mediated Inhibition of PP1γ Activity

Next we tested whether S6K1 regulates URI/PP1γ complex formation via phosphorylation of URI at Ser-371. In this regard, we found that a URI segment corresponding

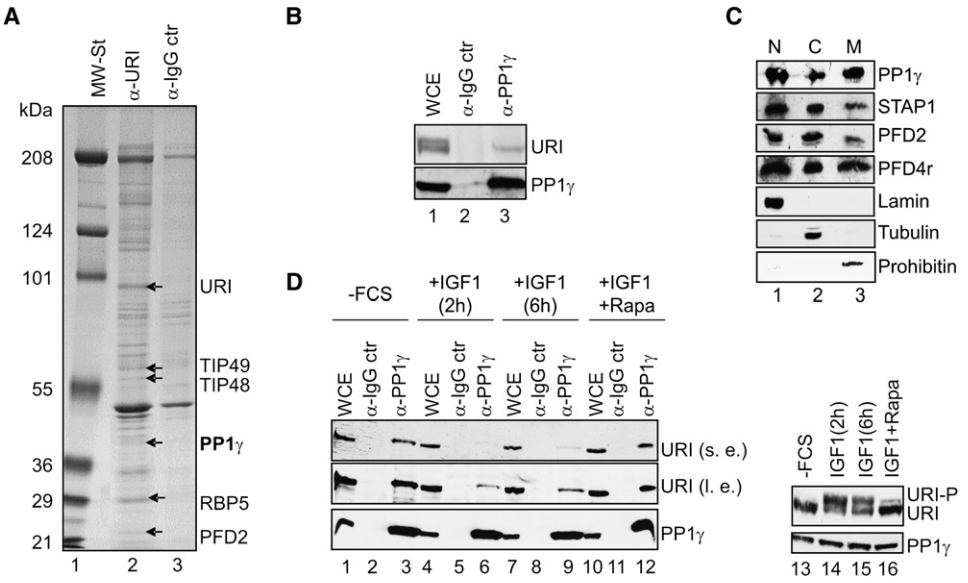

Figure 3. PP1γ Is a URI-Associated Protein that Interacts with URI in a Phosphorylation-Dependent Manner

(A) Immunoprecipitates from serum-starved HEK293 cell lysates with anti-URI mAb mix (58.2, 22.34) (lane 2) or control mouse IgG (lane 3). Lane 1 represents the stained molecular weight marker (MW in kDa).

(B) Whole-cell extracts of HeLa cells (lane 1) were prepared, and aliquots were subjected to immunoprecipitation with control IgG (lane 2) or anti-PP1γ (lane 3) antibodies and immunoblotted for URI and PP1γ.

(C) HeLa cells were processed as in Figure 1M and analyzed by immunoblotting using antibodies against indicated proteins.

(D) HeLa cells were either serum starved (lanes 1–3 and 13) or serum starved and stimulated with IGF1 for indicated times in the absence or presence of rapamycin (lanes 4–12 and 14–16). Aliquots of whole-cell extracts were subjected to immunoprecipitation with anti-PP1γ antibody or control IgG and immunoblotted for URI and PP1γ. Other aliquots were processed directly for immunoblotting with antibody to indicated proteins. URI(s.e.) and (l.e.) denote short and long exposures of the same blot, respectively.

to residues 357–420 is sufficient to mediate interactions with PP1γ in GST pull-down assays (Figure 4A and Figure S8A, lane 6). This segment of URI encompasses residue Ser-371. As shown in Figure 4B, unphosphorylated His_6-URI(WT) bound PP1γ (lane 3). Phosphorylation of His_6-URI(WT) by S6K1 blocked URI/PP1γ complex formation to a significant degree (lane 4). No such inhibition of complex formation was seen when His_6-URI(S371A) mutant protein was exposed to S6K1 kinase reaction (compare lanes 6 and 5). These results establish that S6K1-mediated phosphorylation of URI at Ser-371 is causally linked to the disruption of URI/PP1γ complexes in vitro.

To confirm this result in vivo, we generated retrovirally infected U2OS and HeLa cell pools stably expressing HA-tagged URI(WT) or HA-URI(S371A) mutant species (Figure 4C, lanes 2 and 3). Notably, HA-URI(S371A) migrated faster than wild-type protein, implying that phosphorylation of URI at Ser-371 contributes to the phosphorylation-mediated shift in URI migration. When these cell pools were serum starved and restimulated with IGF1 for various times, the majority of HA-URI(WT) converted to a slower migrating species (Figure 4D, lanes 5 and 6), while the Ser-371 phosphosite mutant species of HA-URI failed to reproduce the same shift (Figure 4D, compare lanes 8 and 9 with lanes 5 and 6). A fraction of HA-URI(S371A) was still converted to a slower migrating form, implying that there are likely additional growth factor-induced phosphorylation site(s) on URI that contribute to the observed changes in the migration of the protein. Importantly, significantly more HA-URI(S371A) coimmunoprecipitated with endogenous PP1γ than with HA-URI(WT) (Figure 4E, compare lanes 4 and 1). Similar results were obtained in HeLa cell pools (data not shown). These results suggest that S6K1-mediated phosphorylation of URI at Ser-371 negatively regulates URI/PP1γ complex formation in vivo.

To assess the functional significance of URI/PP1γ interactions, we asked next whether URI affects PP1γ activity. His_6-URI associated with GST-PP1γ in a dose-dependent manner (Figure 4F). Prior phosphorylation of His_6-URI by His_6-S6K1(WT) blocked, as expected, the binding of His_6-URI to GST-PP1γ (Figure 4F). In parallel, we measured GST-PP1γ-associated phosphatase activity in the absence or presence of increasing amounts of URI. Strikingly, addition of His_6-URI resulted in a dose-dependent inhibition of GST-PP1γ dephosphorylation activity (Figure 4F). Inhibition closely correlated with URI/PP1γ complex formation, implying that unphosphorylated URI, when bound to PP1γ, has the capacity to inhibit enzyme activity. S6K1-phosphorylated His_6-URI did not interact with PP1γ and, likewise, failed to inhibit PP1γ activity (Figure 4F). In accord with these observations, PP1γ immunoprecipitates derived from a mitochondrial fraction

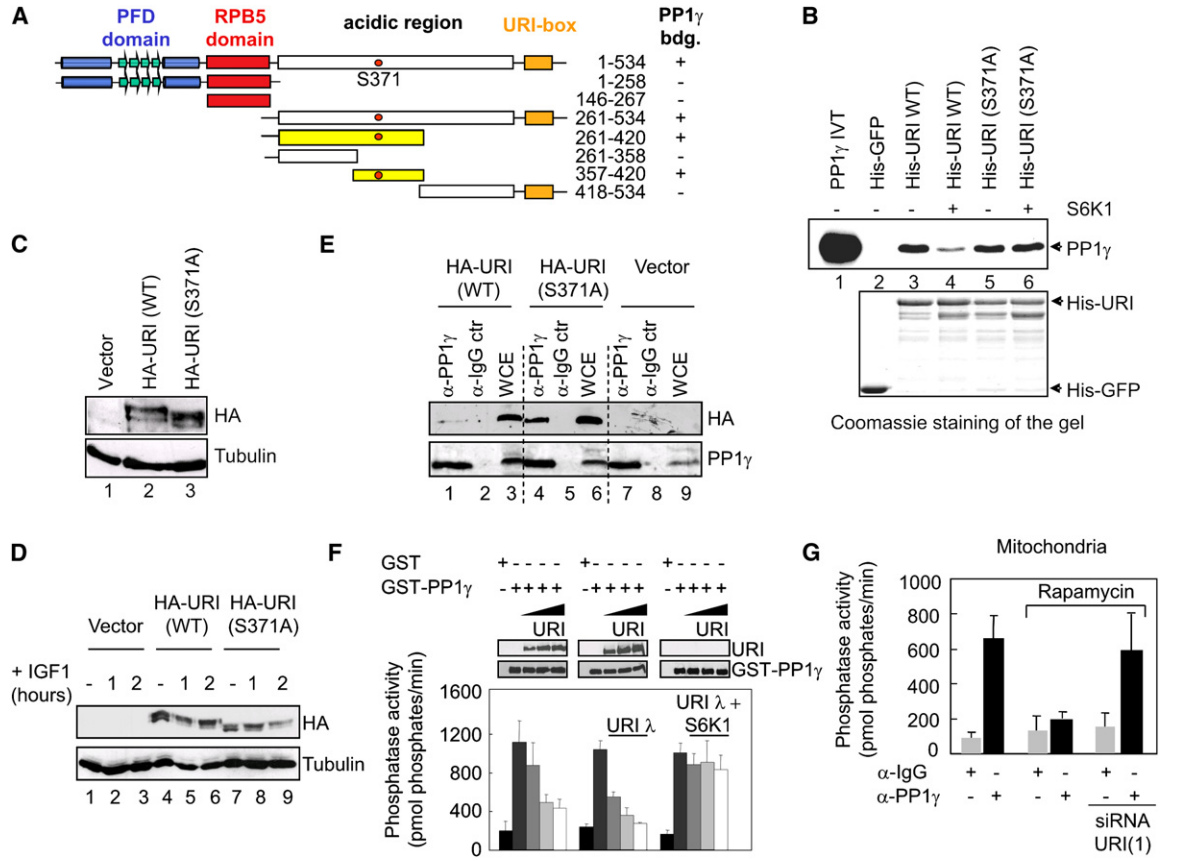

Figure 4. URI Associates with PP1γ via Its C-Terminal Domain and Inhibits PP1γ Activity

(A) Schematic representation of different fragments used in S6K1 phosphorylation and PP1γ binding assays. The yellow fragment indicates the URI fragment phosphorylated by S6K1 that retained PP1γ binding activity. The red spot indicates amino acid Ser-371 in URI phosphorylated by S6K1.

(B) ^{35}S-labeled in vitro-translated PP1γ (lane 1) was incubated with bacterially expressed His-GFP (lane 2), His-URI (WT) (lanes 3 and 4), and His-URI (S371A) (lanes 5 and 6) proteins that had been either not phosphorylated (lanes 2, 3, and 5) or phosphorylated previously with S6K1 (lanes 4 and 6). Coomassie blue staining of the blot (lanes 2–6) is shown.

(C) Characterization of U2OS cell pools. Whole-cell extract aliquots of exponentially growing U2OS cell pools expressing control vector (lane 1), HA-URI (WT) (lane 2), or HA-URI (S371A) (lane 3) were processed directly for immunoblotting with an anti-HA mAb (HA.11) and a tubulin antibody.

(D) U2OS cell pools overexpressing control vector (lanes 1–3), HA-URI (WT) (lanes 4–6), or HA-URI (S371A) (lanes 7–9) were either serum starved (lanes 1, 4, and 7) or serum starved and stimulated with IGF1 for the indicated times (lanes 2 and 3, 5 and 6, and 8 and 9). Whole-cell extracts were prepared as in (C), and aliquots were subjected to immunoblotting against indicated proteins.

(E) Whole-cell extracts of exponentially growing U2OS cell pools expressing either a vector control (lanes 7–9), HA-URI (WT) (lanes 1–3), or HA-URI (S371A) (lanes 4–6) were prepared and subjected to immunoprecipitation with anti-PP1γ antibody or control IgG and immunoblotted against indicated proteins.

(F) Aliquots of glutathione Sepharose preloaded with baculovirus-produced GST or GST-PP1γ fusion proteins were incubated with increasing amounts of either baculovirus-produced His_6-URI, His_6-URI dephosphorylated by λ-phosphatase, or His_6-URI dephosphorylated and rephosphorylated by active S6K1 and processed for PP1γ phosphatase assay (see Experimental Procedures). Other aliquots were processed for immunoblotting for GST-PP1γ-bound URI and GST-PP1γ. Data are represented as mean ± SEM, n = 3.

(G) HeLa cells were either cultured in the absence or presence of rapamycin or were first transfected with URI(1)-siRNA and then treated with rapamycin. Mitochondrial fractions from HeLa cells were directly processed for immunoprecipitation with indicated antibodies followed by phosphatase assays. Data are represented as mean ± SEM, n = 3.

of exponentially growing cells displayed, as expected, significant PP1γ-associated phosphatase activity (Figure 4G). Prior treatment of cells with rapamycin reduced PP1γ-associated phosphatase activity recovered from mitochondria (Figure 4G), while siRNA-mediated knockdown of URI restored rapamycin-mediated inhibition of PP1γ activity (Figure 4G). This suggests that rapamycin-sensitive signaling contributes to the regulation of PP1γ activity at mitochondria in vivo. Immunoblotting confirmed that, in each immunoprecipitate, similar amounts of PP1γ were recovered and that URI-siRNAs depleted efficiently the protein (Figure S8B). Thus, URI acts as an inhibitor of PP1γ at mitochondria and phosphorylation of URI by S6K1 at Ser-371 triggers the disruption of URI/PP1γ complexes, thereby freeing PP1γ from inhibition by bound URI.

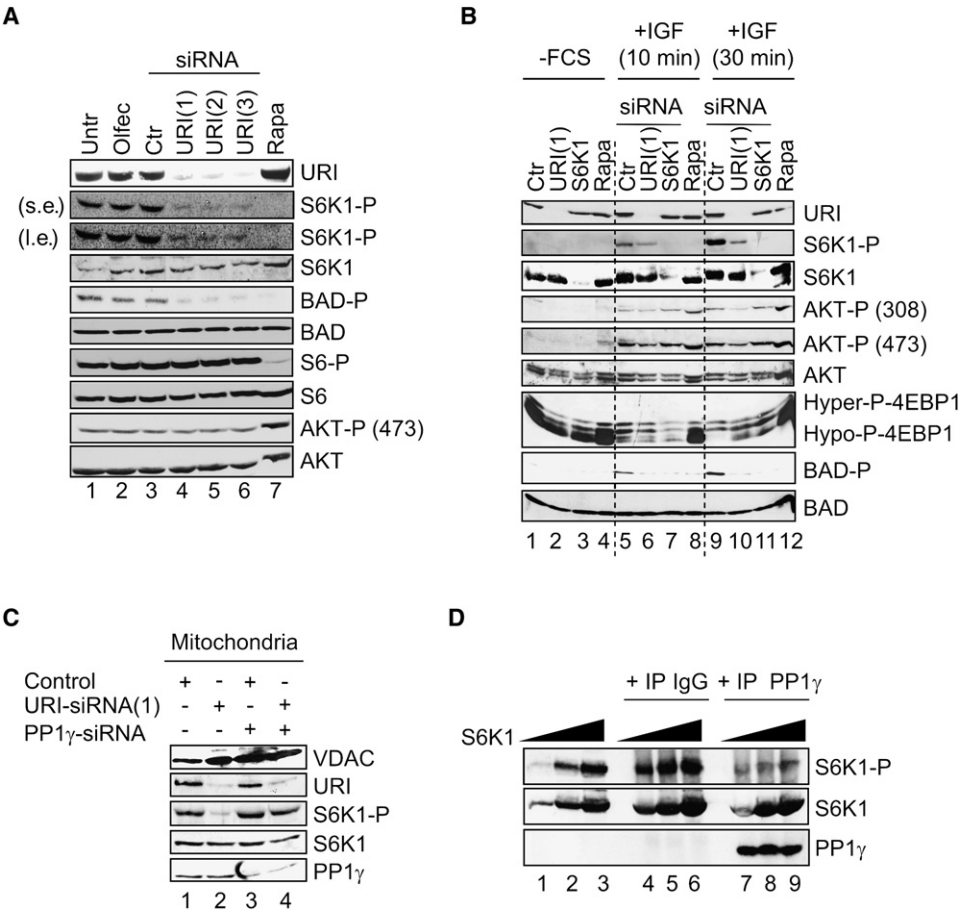

Figure 5. URI and PP1γ Regulate S6K1 Activation State and BAD Phosphorylation

(A) siRNAs corresponding to the mRNAs for the indicated proteins were transfected in HeLa cells, and lysates were analyzed for amounts of URI, phospho-(P), and total S6K1, BAD, S6 and AKT. Lysates of untransfected (untr) (lane 1), transfection reagent-treated (olfec) (lane 2), control siRNA-transfected (ctr) (lane 3), or rapamycin-treated (rapa) (lane 7) HeLa cells served as controls. URI(1), (2), and (3) indicate different siRNAs targeting *URI* mRNAs (lanes 4–6).

(B) HeLa cells were either rapamycin treated (lanes 4, 8, and 12) or transfected with indicated siRNAs (lanes 1–3, 5–7, and 9–11), serum starved (lanes 1–4), or serum starved and stimulated with IGF1 for the indicated times (lanes 5–12). Lysates were analyzed as in (A).

(C) HeLa cells were transfected with control siRNAs (lanes 1 and 3), URI(1)-siRNAs (lanes 2 and 4), and PP1γ-siRNAs (lanes 3 and 4), and mitochondrial subfraction-derived lysates were analyzed as in (A).

(D) Mitochondrial lysates from U2OS cells were directly processed for immunoprecipitation with indicated antibodies (IgG and PP1γ), and immunoprecipitates were subjected to phosphatase assay in presence of increased concentrations of baculovirus-produced S6K1. Reactions were subjected to immunoblotting against indicated proteins.

Knockdown of URI Causes Attenuation of S6K1 Activity in a PP1γ-Dependent Manner

To explore the biochemical consequences of releasing the PP1γ pool normally bound to URI, we depleted URI using three different sets of siRNAs. Knockdown of URI in HeLa cells resulted in downregulation of Thr-389 phosphorylation of S6K1, an indicator for active S6K1 (Figure 5A, lanes 4–6). S6K1 immunoprecipitates derived from URI knockdown cells also displayed low associated kinase activity compared to those from wild-type cells (Figure S9A, compare lanes 3 and 1). Phosphorylation of BAD at Ser-136 was also diminished (Figure 5A). Similar effects were seen in U2OS cells (Figure S9B). In contrast, Ser-473 phosphorylation of Akt/PKB remained largely unaffected in URI-siRNA-treated cells (Figure 5A, lanes 4–6), implying that knockdown of URI affects specifically the S6K1-BAD signaling axis at mitochondria. Knockdown of URI also failed to substantially reduce S6 phosphorylation (Figure 5A, lanes 4–6), consistent with previous work implying a role for S6K2 in mediating S6 phosphorylation (Pende et al., 2004).

Finally, URI knockdown also blunted S6K1 activation in response to short-term IGF1 stimulation of serum-starved HeLa cells (Figure 5B). Knockdown of URI did not affect to a considerable extend the phosphorylation state of Akt/PKB as monitored by the phosphorylation state of Ser-473 and Thr-308 and of the translational inhibitor 4E-BP1 (Figure 5B). As expected, phosphorylation of the

latter upon IGF1 stimulation was efficiently blocked by rapamycin (Figure 5B). However, URI knockdown profoundly affected the phosphorylation of BAD on Ser-136 following IGF1 stimulation (Figure 5B). Similar results were observed in HeLa cells that had been serum-starved and restimulated with IGF1 for a longer time period (Figure S9C). These results establish a key role for URI in maintaining S6K1 signaling and BAD phosphorylation under normal growth conditions and in response to IGF1 stimulation.

To test whether URI's effect on S6K1 and BAD is directly linked to PP1γ function, we treated URI knockdown cells with calyculin, a serine/threonine phosphatase inhibitor. Downregulation of URI caused substantial inhibition of Thr-389 and Ser-136 phosphorylation of S6K1 and BAD, respectively (Figure S9D, lane 2). Calyculin prevented this (Figure S9D, lane 4). We also codepleted PP1γ and URI with siRNAs and measured S6K1 Thr-389 phosphorylation in mitochondrial fractions. Efficient depletion of PP1γ in cells lacking URI restored S6K1 Thr-389 phosphorylation (Figure 5C, lane 4). Downregulation of PP1γ alone had no such effect on S6K1 activation state (Figure 5C). These results suggest that at least one consequence of URI knockdown is the release of PP1γ, which in turn mediates downregulation of S6K1 activity and diminished Ser-136 phosphorylation of BAD.

To test a potential role for PP1γ in mediating directly the dephosphorylation of S6K1 at Thr-389, we incubated active His_6-S6K1 with PP1γ immunoprecipitates derived from mitochondrial fractions of U2OS cells. Strikingly, PP1γ dephosphorylated Thr-389 of S6K1 with high efficiency, as evidenced by immunoblotting of S6K1 with anti-phospho-Thr-389 antibodies (Figure 5D, lanes 7–9). Control immunoprecipitates displayed no such dephosphorylation activity directed toward S6K1 (Figure 5D, lanes 4–6). Thus, mitochondrial PP1γ can function as an S6K1 phospho-Thr-389 phosphatase, consistent with a model in which phosphorylation of URI at Ser-371 by S6K1 releases PP1γ, which in turn restricts S6K1 activity, one consequence of which is a decline in BAD phosphorylation.

Knockdown of URI Induces Cell Death in a PP1γ-Dependent Manner

Given that S6K1 mediates survival signaling, at least in part, by phosphorylating BAD at Ser-136 and the fact that knockdown of URI restricts S6K1 signaling in a PP1γ-dependent manner, we determined whether depletion of URI affects cell survival. Knockdown of URI decreased the number of actively dividing cells as compared to control cells (Figure 6A). Concomitantly, we observed an increase in the number of cells with a sub-G1 DNA content (Figure 6B). Similar effects were seen after downregulation of S6K1 (Figures 6A and 6B). We also observed PARP cleavage in URI or S6K1 knockdown cells (Figure S10A, lanes 4–7). Moreover, six different siRNAs targeting S6K1 mRNAs, each highly efficient in downregulating S6K1, caused PARP cleavage (Figure S11A) and induced cell death that was most apparent at 72 hr following downregulation of S6K1 (Figure S11B). No such changes were observed in either control siRNA- or oligofectamine-treated cells (Figures 6A and 6B and Figures S10A and S11B). Finally, microscopic examination of URI- or S6K1-depleted cells revealed that a significant fraction of these cells were small and had rounded up and detached from the culture dish at the 72 hr time point (Figures S10E–S10J and S10N). Rapamycin did not have such an effect (Figures S10K–S10M). Depletion of either URI or S6K1 increased also the amounts of BAD present at mitochondria and induced release of cytochrome *c* at the 48 hr and 72 hr, but not at the 24 hr, time point (Figure 6C). Combined, this cell biological and biochemical evidence suggests that URI function is critical to suppress cell death under normal growth conditions.

To test whether cell death caused by depletion of URI is PP1γ dependent, both were downregulated in combination, which prohibited cell death (Figure 6G), reduced the accumulation of BAD at mitochondria, and prevented cytochrome *c* release (Figure 6H, compare lanes 4 and 2). Knockdown of PP1γ alone did not enhance cell death (Figure 6F). Thus, cell death triggered by loss of URI is PP1γ dependent.

Because BAD phosphorylation determines, at least in part, the level of mitochondrial apoptotic input to which a cell has to be exposed in order to undergo apoptosis, we downregulated URI in serum-starved cells, a setting where URI/PP1γ complexes are highly abundant and where growth factor-stimulated BAD phosphorylation is reduced. As one would predict from our model, serum-starved cells responded to knockdown of URI with an increased apoptotic response compared to exponentially growing cells (Figure S10, compare [R] and [Q]), providing additional support that URI functions, at least in part, by protecting cells from the deleterious effects of growth factor deprivation.

The above-noted results show that knockdown of URI decreases the number of actively dividing cells, at least in part by promoting cell death in a PP1γ-dependent manner. Given that phosphorylation of URI at Ser-371 negatively regulates PP1γ binding in vivo (see Figure 4E), we compared proliferation of U2OS cell pools stably expressing HA-URI(WT) with that of HA-URI(S371A) mutant species. As illustrated in Figure 6I, U2OS cells expressing the Ser-371 phosphosite mutant of URI increased their cell number over time more rapidly than vector control cells or cells expressing wild-type protein. Similar results were obtained in HeLa cells stably expressing the wild-type and Ser-371 phosphosite mutant species of URI (Figure S10S). These results imply that at least one consequence of phosphorylating URI at Ser-371 is to release PP1γ from bound URI in order to prevent an excessive increase in cell number. In this regard, Thr-389 phosphorylation of S6K1 was enhanced in HA-URI(S371A)-expressing cells after IGF1 stimulation as compared to wild-type control cells (Figure 6J).

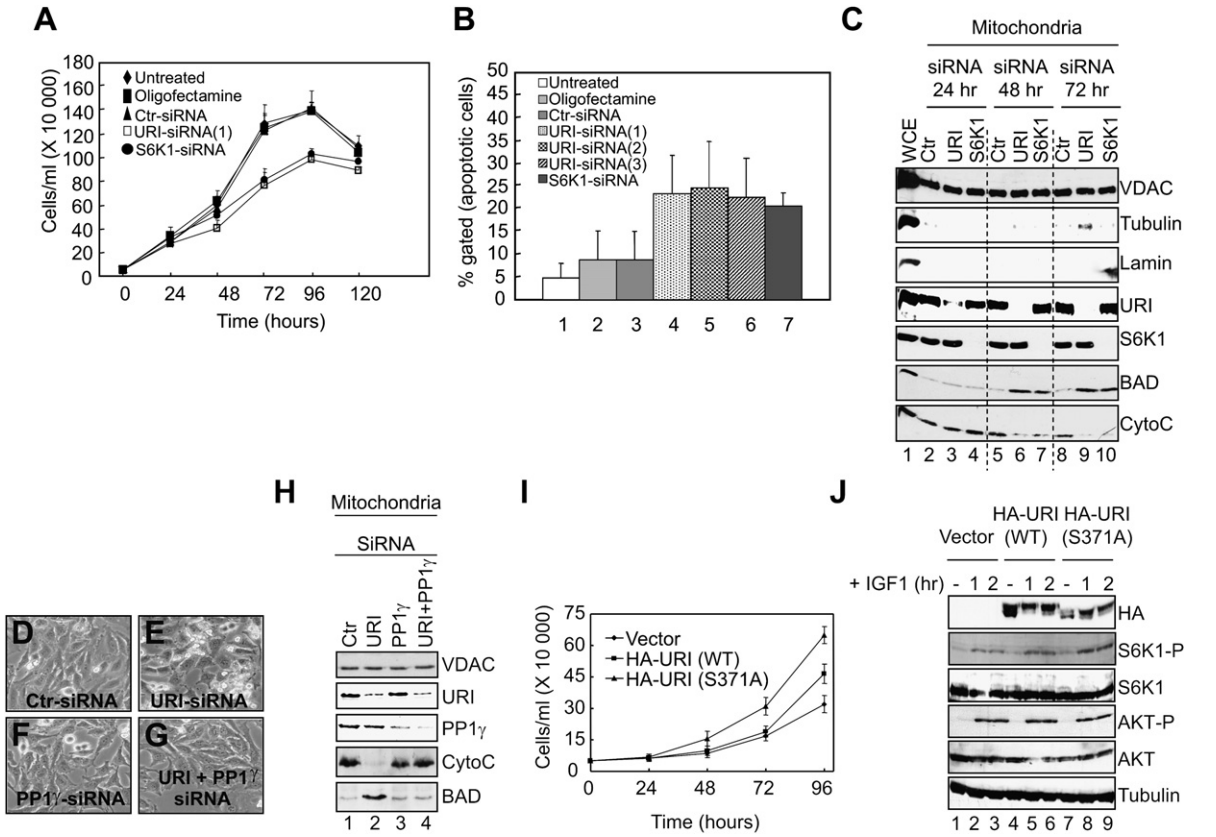

Figure 6. URI Function Is Required to Suppress PP1γ-Mediated Apoptosis

(A) HeLa cells were either not transfected (full diamond), treated with transfection reagent (full square), or transfected with ctr-siRNA (full triangle), URI-siRNA(1) (open square), or S6K1(1)-siRNA (full circle), and cell numbers were determined over the indicated time period. An average of three independent experiments is shown. Data are represented as mean ± SEM, n = 3.

(B) HeLa cells were either not transfected (lane 1), treated with transfection reagent (lane 2), or transfected with ctr-siRNA (lane 3), URI-siRNA(1) (lane 4), URI-siRNA(2) (lane 5), URI-siRNA(3) (lane 6), or S6K1(1)-siRNA (lane 7) and analyzed for sub-G1 DNA content after 72 hr by fluorescence-activated cell sorting. Data are represented as mean ± SEM, n = 3.

(C) HeLa cells were transfected with indicated siRNAs (lanes 2–10) for the indicated times, and mitochondrial subfractions were prepared and processed for immunoblotting with antibodies against indicated proteins. WCE (lane 1) denotes whole-cell extracts of untreated HeLa cells.

(D–G) HeLa cells were transfected with siRNAs corresponding to the mRNAs for the indicated proteins and examined by light microscopy at 72 hr posttransfection. Representative phase-contrast micrographs of cells are shown.

(H) Mitochondria from HeLa cells were processed as in (C). HeLa cells were transfected with indicated siRNAs (lanes 1–4) for 72 hr, and mitochondrial fractions were prepared and processed for immunoblotting with antibodies against indicated proteins.

(I) Determination of cell number over time of U2OS cell pools expressing a control vector (full diamond), HA-URI (WT) (full square), and HA-URI (S371A) (full triangle). An average of three independent experiments is shown. Data are represented as mean ± SEM.

(J) U2OS cell pools expressing a control vector (lanes 1–3), HA-URI (WT) (lanes 4–6), or HA-URI (S371A) (lanes 7–9) were either serum starved (lanes 1, 4, and 7) or serum starved and stimulated with IGF1 for the indicated times (lanes 2 and 3, 5 and 6, and 8 and 9). Whole-cell extracts were prepared as in (C), and aliquots were subjected to immunoblotting against indicated proteins.

Importantly, Ser-473 phosphorylation of Akt/PKB did not change under these experimental conditions (Figure 6J). These results argue that Ser-371 phosphorylation of URI triggers PP1γ release, which in turn engages a negative feedback that diminishes S6K1 activity, thereby preventing sustained S6K1 signaling.

Cell Death Triggered by Loss of URI Is BAD Dependent

Thus far, our results point to a key role for URI in the suppression of cell death mediated in part via inhibition of PP1γ function that, when unleashed, affects S6K1-BAD signaling and thus cell death responses. To assess whether BAD function is in fact required for cell death caused by loss of URI function, we depleted URI in mouse embryonic fibroblasts (MEFs) deficient for BAD (Ranger et al., 2003). Two distinct sets of lentiviruses expressing shRNAs directed toward mouse *URI* mRNAs depleted efficiently URI in wild-type and *BAD*$^{-/-}$ MEFs (Figure 7A, lanes 3 and 4 and 5 and 6, respectively). Knockdown of URI in wild-type MEFs caused, like in human cells, cell death (Figures 7D and 7F). In contrast, little cell death

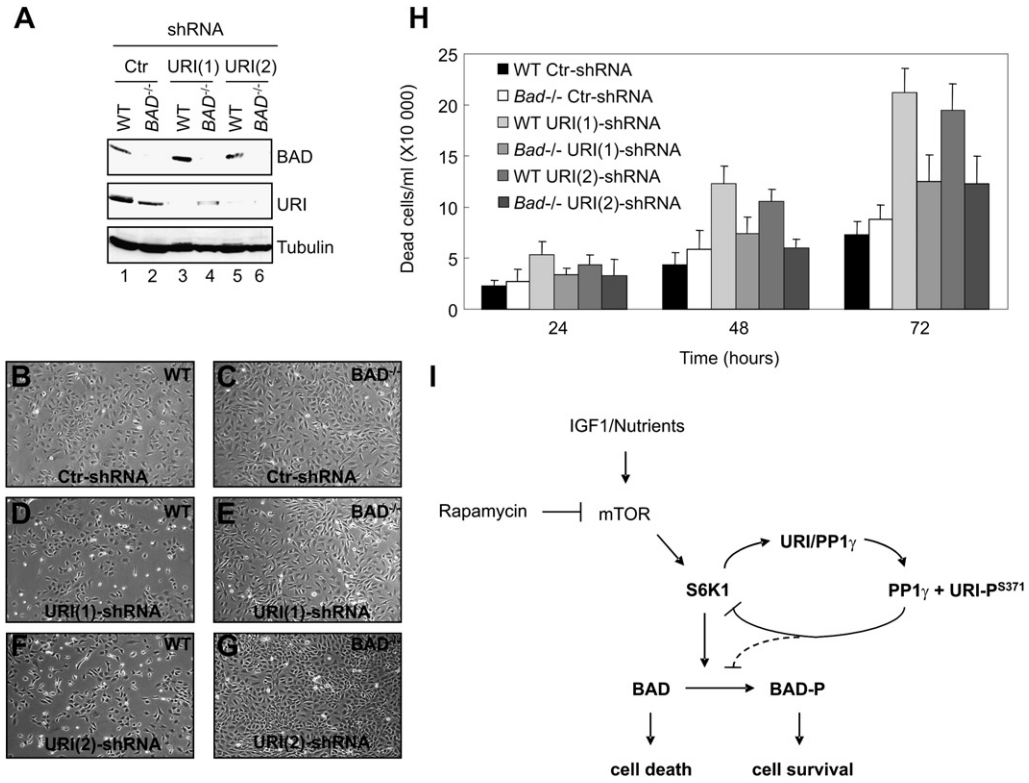

Figure 7. URI-Mediated Cell Death Requires BAD

(A) Wild-type MEFs and MEFs deficient for BAD were infected with ctr-shRNA (lanes 1 and 2), URI-shRNA(1) (lanes 3 and 4), and URI-shRNA(2) (lanes 5 and 6) lentiviruses, and whole-cell extracts were subjected to immunoblotting with antibodies against indicated proteins.

(B–G) Wild-type MEFs (B, D, and F) and BAD-deficient MEFs (C, E, and G) were infected with ctr-shRNAs (B and C), URI-shRNA(1) (D and E), or URI-shRNA(2) (F and G) lentiviruses and examined by light microscopy at 72 hr posttransfection. Representative phase-contrast micrographs of cells are shown.

(H) Wild-type MEF cells and BAD-deficient MEFs were infected with ctr-shRNA, URI-shRNA(1), or URI-shRNA(2) lentiviruses, and apoptotic cells were quantified with a trypan blue staining at the indicated time postinfection. Data are represented as mean ± SEM, n = 3.

(I) Model proposing a role for URI and PP1γ as central components of a negative feedback mechanism that counteracts S6K1 survival signaling to BAD in response to growth factors (for details see Discussion).

was observed following downregulation of URI in *BAD*$^{-/-}$ MEFs (Figures 7E and 7G). Control siRNAs had no such effects (Figures 7B and 7C). Quantification of cell death in wild-type and *BAD*$^{-/-}$ MEFs at various times following URI depletion confirmed that the latter are significantly more resistant to cell death caused by URI depletion than the former (Figure 7H). These results establish a key role for BAD in a cell death pathway induced by loss of URI.

DISCUSSION

This study demonstrates that the unconventional member of the PFD family URI coexists with PP1γ in a stable mitochondrial complex and forms an integral part of a homeostatic signaling mechanism involved in setting the mitochondrial threshold for apoptosis in accord with growth factor and nutritional signals conveyed via the mTOR-S6K1 signaling axis. We postulate the following model of how dynamic regulation of mitochondria-localized URI/PP1γ complexes by S6K1-mediated URI phosphorylation affects survival signaling (Figure 7I).

Under growth factor-deprived conditions or in the presence of rapamycin, URI is bound to PP1γ at mitochondria and inhibits the activity of the bound phosphatase. Growth factor stimulation leads to dissociation of URI/PP1γ complexes in a rapamycin-sensitive manner, supporting the view that mitochondrial URI/PP1γ interactions are regulated by mTOR signaling. S6K1 acts downstream of mTOR and, as shown here, can directly phosphorylate URI at Ser-371, causing disassembly of URI/PP1γ complexes. We propose that this event enhances the active pool of PP1γ at mitochondria. Accordingly, URI acts as a natural inhibitor of PP1γ at mitochondria and the extent to which URI is phosphorylated at Ser-371 by S6K1 (which is a function of available nutrients and growth factors) determines how much PP1γ is set free and active.

What might be the target(s) of URI-liberated PP1γ at mitochondria? Knockdown of URI results in diminished S6K1 activity and BAD phosphorylation at Ser-136. It is

therefore tempting to consider a specific role for mitochondrial PP1γ in attenuating S6K1 activity. Supporting this view is the finding that PP1γ immunoprecipitates recovered from mitochondrial lysates displayed potent S6K1 Thr-389 dephosphorylation activity. In addition, loss-of-URI-mediated inhibition of S6K1 activity is salvaged by knockdown of PP1γ. Therefore, PP1γ may function, when released from URI, as part of a negative feedback mechanism that operates at mitochondria to restrict, at least in part, S6K1 activity, thereby protecting the cell from the potential deleterious effects of sustained S6K1 signaling, such as enhanced resistance of cells to undergo apoptosis in response to death cues. Additionally, there is evidence that PP1γ can dephosphorylate BAD directly (Danial et al., 2003). It is reasonable to consider that URI-liberated PP1γ contributes through both S6K1-dependent and -independent routes to the dephosphorylation of BAD, thereby enhancing the cell's susceptibility to undergo apoptosis. The mechanism described here provides therefore an efficient means to counter the prosurvival effects of the multiple growth factor-induced kinase pathways impinging on BAD, the end product of which is a lowered mitochondrial threshold for cell death. Thus, phosphorylation-dependent regulation of URI/PP1γ interactions by S6K1 serves a critical role in setting a proper mitochondrial threshold for apoptosis under homeostatic conditions and in response to growth stimuli.

Unlike URI depletion, treatment of cells with rapamycin did not lead to cell death despite the fact that each treatment led to dephosphorylation and inactivation of S6K1. We note, however, that in the presence of rapamycin, PP1γ is bound to URI at mitochondria and is thus inactive. Indeed, we were unable to recover significant PP1γ-associated phosphatase activity from mitochondrial fractions of cells treated with rapamycin (see Figure 4G). Hence, there is a fundamental difference between inactivation of S6K1 through blocking mTOR function and negative feedback activation through disruption of URI/PP1γ complexes. This difference may be based on the fact that rapamycin treatment affects all mTOR-dependent effector pathways simultaneously, whereas depletion of URI unleashes PP1γ at mitochondria, leading to the selective inhibition of mitochondria-resident S6K1. Finally, there is evidence to suggest that serum or IGF1 treatment protects against rapamycin-induced elevation of JNK signaling that, in turn, promotes apoptosis in p53-deficient cells (Huang et al., 2003). This suggest that growth factors and genetic make-up can influence a cell's response to rapamycin. Because the experiments described here have been performed in the presence of serum or IGF1, it is not unexpected that we failed to observe cell death in response to rapamycin. Further work will be required to determine the various factors influencing a cell's response to rapamycin.

Our results also suggest that S6K1 performs a key survival function at mitochondria, as evidenced by the observation that depletion of it leads to cell death. This observation is consistent with several other reports describing a requirement of S6K1 for cell survival in multiple different cell systems (Freilinger et al., 2006; Harada et al., 2001; Wu et al., 2004). Therefore, in addition to its well-established role in growth control, S6K1 serves an equally important function in delivering survival signals in different cell types, at least in part, by phosphorylating BAD at Ser-136. The same site in BAD has also been shown to be phosphorylated by Akt/PKB (Datta et al., 1997). The existence of distinct BAD Ser-136 kinases suggests that cellular context and/or activation states of signal transduction pathways may contribute to which extent one or the other kinase (or both) mediates phosphorylation of BAD on Ser-136.

In summary, the results presented here define a functional mitochondrial signaling network involving S6K1, URI, PP1γ, and BAD. At the heart of this network is a homeostatic mechanism that protects cells from the consequences of sustained S6K1 survival signaling to BAD, thereby helping to set the cell's mitochondrial threshold for death in accord with the availability of nutrients and growth factors. Because many diseases are the result of homeostatic imbalances and negative feedback programs are predominant mechanisms for homeostatic control, it will be interesting to determine whether certain tumor cells have undergone mutations in pathways that make URI/PP1γ complexes less amenable to disruption in response to upstream signaling. Such mechanism, if existent, could contribute to tumor cell evolution by increasing the resistance of cells to death cues. Conversely, agents that would be able to disrupt URI/PP1γ complexes might enhance the sensitivity of tumor cells to death cues and thus be useful in tumor cell killing.

EXPERIMENTAL PROCEDURES

Cell Culture, Transfection, FACS Analysis, Proliferation, and Cell Death Assays

HeLa, HEK293, U2OS, wild-type, and corresponding BAD-deficient MEFs (kind gift from Andreas Strasser) were cultivated in DMEM supplemented with 10% fetal calf serum. HeLa and HEK293 cells were transiently transfected using the $CaCl_2$ method and harvested ~24 hr after removal of the precipitate. siRNAs were transfected following a double-transfection protocol using oligofectamine (Invitrogen) according to the procedures of the manufacturer. For sub-G1 DNA content analysis, HeLa cells were processed for flow cytometric analysis (FACS) as described (Krek and Nigg, 1991). Cell proliferation capacity of various siRNA-transfected cultures was determined by seeding cells in series of culture dishes at 30% confluency and cultivating them for several days. Apoptotic cells were quantified with trypan blue staining. Cells were counted every 24 hr with a hemacytometer. For each culture, the cell number at each time point reflects the average of data from three dishes.

Retroviral and Lentiviral Infections

Retroviruses were produced by transfection of the LinX packaging cell line with pBABE-puro vectors, and supernatants were used to infect HeLa and U2OS cells. Stable pools were generated by selection for 10 days in the presence of 5 μg/ml of puromycin. Lentiviruses for knockdown of URI in MEFs were from Sigma, Mission Lentiviral

Transduction Particles. URI-shRNA(1) (clone ID, TRCN0000095384) and URI-shRNA(2) (clone ID, TRCN0000095386) were used to infect MEFs (WT) and BAD-deficient MEFs in the presence of 8 μg/ml of polybrene for 72 hr. Control lentivirus particles were produced by transfection of HEK293 cells with the vectors psPAX2, pMD2G (kind gift of Didier Trono, EPFL, Lausanne), and pLKO-1-ns (Addgene clone 10879). Apoptotic cells (using trypan blue exclusion) were quantified every 24 hr with a hemacytometer. For each culture, the cell number at each time point reflects the average of data from three dishes.

Plasmids, siRNAs, Recombinant Protein Expression, and Immunological Techniques

Details of plasmid constructions and siRNA sequences as well as the procedures for expression of recombinant proteins in bacteria and Sf9 insect cells are provided in the Supplemental Experimental Procedures. Immunoblotting and immunoprecipitations were performed as described (Hergovich et al., 2003).

Antibodies and Reagents

Antibodies recognizing STAP1 (mAb 105.128), PFD2, PFD4r, and URI (mAb 58.2) have been described previously (Gstaiger et al., 2003). Rabbit polyclonal antibody directed toward a C-terminal part of URI was raised against GST-URI (418–534) fusion proteins, referred to as anti-URI(Ct), and affinity-purified as described (Gstaiger et al., 2003). Anti-S6K1, anti-S6, anti-S6 (pSer-240/244), anti-AKT, anti-AKT (pSer-473), and anti-BAD (pSer-136) were from Cell Signaling Technology. Anti-BAD was from BD Transduction Laboratories. Anti-lamin, anti-tubulin, anti-prohibitin, anti-VDAC, anti-PP1γ, anti-AKT (pThr-308), anti-S6K1 (pThr-389), and anti-βTrCP were purchased from Santa Cruz. Anti-cox IV and anti-cytochrome *c* were from BD Biosciences Pharmingen. Mouse monoclonal antibodies anti-Myc (9E10) and anti-HA (11) were from Abcam and Babco, respectively. The antibodies anti-GST and anti-Flag (M2) were from Sigma. Recombinant human IGF1 was obtained from R&D Systems and used at a concentration of 50 ng/ml. Rapamycin was from Calbiochem and was applied at a concentration of 50 nM for 5 hr. Calyculin was obtained from Sigma and used at the concentration of 10 nM for 20 min.

Immunofluorescence Microscopy

Exponentially growing HeLa cells were plated on coverslips and processed for indirect immunofluorescence microscopy using a paraformaldehyde/Triton X-100 procedure as described (Hergovich et al., 2003). Secondary antibodies included donkey anti-rabbit fluorescein isothiocyanate (FITC) and anti-mouse Texas red (Jackson Immunoresearch, West Grove, PA). For labeling of mitochondria, cells were incubated with MitoTracker (M-7512; Molecular Probes, Eugene, OR) for 30 min at a final concentration of 100 nM before fixation. Coverslips were then inverted into 5 ml Vectashield medium (Vector Lab, Burlingare, CA). Images were obtained with a Fluoview FV500 confocal laser scanning microscope (Olympus, Melville, NY). Photographic images were processed using Photoshop 5.0 (Adobe Systems, San Jose, CA).

Subcellular Fractionation

HeLa cells were resuspended in a fractionation buffer containing 70 mM sucrose, 220 mM mannitol, and 10 mM HEPES (pH 7.4) supplemented with protease inhibitors and lysed by 50 strokes with Dounce homogenizer using a B pestle. Homogenization was checked by phase-contrast microscopy. After centrifugation at 800 × g for 5 min at 4°C, the pellet, which represents the nuclear fraction, was resuspended in RIPA buffer (10 mM Tris [pH 7.5], 100 mM NaCl, 1 mM EDTA, 1 mM EGTA, 1 mM NaF, 20 mM $Na_4P_2O_7$, 2 mM Na_3VO_4, 0.1% SDS, 0.5% sodium deoxycholate, 1% Triton X-100, and 10% glycerol) supplemented with protease inhibitors. The supernatant was immediately centrifuged at 8000 × g for 20 min at 4°C to obtain a mitochondria-enriched pellet fraction and the cytoplasmic fraction in the supernatant. The mitochondria pellet fraction was washed three times with fractionation buffer and resuspended in RIPA buffer. Protein concentrations of the fractions were determined (DC Protein Assay, Bio-Rad Laboratories). To determine the mitochondrial localization, pellets enriched in mitochondria were treated with increasing concentrations of Proteinase K (0.01–50 μg/μl) on ice for 30 min. The reaction mixture was spun at 8000 × g for 20 min at 4°C, and pellets were collected and dissolved in SDS-lysis buffer.

Identification of URI-Associated Proteins and Phosphosites by Mass Spectrometry

Identification of URI-associated proteins in serum-starved cells was done by mass spectrometry as described (Yart et al., 2005). Details for identification and quantification of phosphosites by quantitative mass spectrometry are provided in the Supplemental Experimental Procedures.

In Vitro Phosphatase and Kinase Assays

Phosphatase assays were performed using the Upstate Biotechnology kit with immunoprecipitated URI/PP1γ complexes from mitochondrial fractions of HeLa cells or baculovirus-expressed recombinant GST-PP1γ. For λ-phosphatase (λPPase) treatment, the respective GST or His_6 recombinant proteins were pretreated with 100 units of λPPase in presence of phosphatase buffer containing 50 mM Tris-HCl (pH 7.5), 250 mM NaCl, 0.1 mM EDTA, 0.5% NP-40, 5 mM DTT, and 2 mM $MnCl_2$ for 30 min at 30°C. Details of in vitro kinase reactions including all buffer compositions are provided in the Supplemental Experimental Procedures.

In Vitro Binding Reactions

Baculovirus-expressed GST, GST-PP1γ, and GST-URI were purified on glutathione Sepharose beads and incubated with ^{35}S-methionine-labeled in vitro translation products of either URI or PP1γ generated by the TNT system (Promega). Bound proteins were analyzed on SDS-PAGE and detected by fluorography.

Supplemental Data

Supplemental Data include eleven figures, Supplemental Experimental Procedures, and Supplemental References and can be found with this article online at http://www.molecule.org/cgi/content/full/28/1/28/DC1/.

ACKNOWLEDGMENTS

We thank all members of our lab for helpful discussions and G. Thomas (Cincinnati) for myc-S6K1 (WT) and myc-S6K1 (KD) mammalian expressing plasmids, and baculovirus encoding His_6-S6K1; M. Beullens (Leuven, Belgium) for rat PP1γ cDNA; and D. Huang and A. Strasser (both WIHI, Australia) for BAD-deficient MEFs. We are particularly thankful to I. Frew, D. Plas, and G. Thomas for critical reading of the manuscript. A.S. has been supported by the Roche/CC-SPMD Consortium. This work has been supported by a Collaborative Cancer Research Project Grant of Oncosuisse to W.K.

Received: August 9, 2006
Revised: April 27, 2007
Accepted: August 13, 2007
Published: October 11, 2007

REFERENCES

Bergmann, A. (2002). Survival signaling goes BAD. Dev. Cell *3*, 607–608.

Danial, N.N., Gramm, C.F., Scorrano, L., Zhang, C.Y., Krauss, S., Ranger, A.M., Datta, S.R., Greenberg, M.E., Licklider, L.J., Lowell, B.B., et al. (2003). BAD and glucokinase reside in a mitochondrial complex that integrates glycolysis and apoptosis. Nature *424*, 952–956.

Datta, S.R., Dudek, H., Tao, X., Masters, S., Fu, H., Gotoh, Y., and Greenberg, M.E. (1997). Akt phosphorylation of BAD couples survival signals to the cell-intrinsic death machinery. Cell *91*, 231–241.

Datta, S.R., Katsov, A., Hu, L., Petros, A., Fesik, S.W., Yaffe, M.B., and Greenberg, M.E. (2000). 14-3-3 proteins and survival kinases cooperate to inactivate BAD by BH3 domain phosphorylation. Mol. Cell *6*, 41–51.

Datta, S.R., Ranger, A.M., Lin, M.Z., Sturgill, J.F., Ma, Y.C., Cowan, C.W., Dikkes, P., Korsmeyer, S.J., and Greenberg, M.E. (2002). Survival factor-mediated BAD phosphorylation raises the mitochondrial threshold for apoptosis. Dev. Cell *3*, 631–643.

Freilinger, A., Rosner, M., Krupitza, G., Nishino, M., Lubec, G., Korsmeyer, S.J., and Hengstschlager, M. (2006). Tuberin activates the proapoptotic molecule BAD. Oncogene *25*, 6467–6479.

Gstaiger, M., Luke, B., Hess, D., Oakeley, E.J., Wirbelauer, C., Blondel, M., Vigneron, M., Peter, M., and Krek, W. (2003). Control of nutrient-sensitive transcription programs by the unconventional prefoldin URI. Science *302*, 1208–1212.

Hammerman, P.S., Fox, C.J., and Thompson, C.B. (2004). Beginnings of a signal-transduction pathway for bioenergetic control of cell survival. Trends Biochem. Sci. *29*, 586–592.

Harada, H., Andersen, J.S., Mann, M., Terada, N., and Korsmeyer, S.J. (2001). p70S6 kinase signals cell survival as well as growth, inactivating the pro-apoptotic molecule BAD. Proc. Natl. Acad. Sci. USA *98*, 9666–9670.

Hergovich, A., Lisztwan, J., Barry, R., Ballschmieter, P., and Krek, W. (2003). Regulation of microtubule stability by the von Hippel-Lindau tumour suppressor protein pVHL. Nat. Cell Biol. *5*, 64–70.

Huang, S., Shu, L., Dilling, M.B., Easton, J., Harwood, F.C., Ichijo, H., and Houghton, P.J. (2003). Sustained activation of the JNK cascade and rapamycin-induced apoptosis are suppressed by p53/p21(Cip1). Mol. Cell *11*, 1491–1501.

Klumpp, S., and Krieglstein, J. (2002). Serine/threonine protein phosphatases in apoptosis. Curr. Opin. Pharmacol. *2*, 458–462.

Krek, W., and Nigg, E.A. (1991). Differential phosphorylation of vertebrate p34cdc2 kinase at the G1/S and G2/M transitions of the cell cycle: identification of major phosphorylation sites. EMBO J. *10*, 305–316.

Martin-Benito, J., Boskovic, J., Gomez-Puertas, P., Carrascosa, J.L., Simons, C.T., Lewis, S.A., Bartolini, F., Cowan, N.J., and Valpuesta, J.M. (2002). Structure of eukaryotic prefoldin and of its complexes with unfolded actin and the cytosolic chaperonin CCT. EMBO J. *21*, 6377–6386.

Pende, M., Um, S.H., Mieulet, V., Sticker, M., Goss, V.L., Mestan, J., Mueller, M., Fumagalli, S., Kozma, S.C., and Thomas, G. (2004). S6K1(−/−)/S6K2(−/−) mice exhibit perinatal lethality and rapamycin-sensitive 5′-terminal oligopyrimidine mRNA translation and reveal a mitogen-activated protein kinase-dependent S6 kinase pathway. Mol. Cell. Biol. *24*, 3112–3124.

Plas, D.R., and Thompson, C.B. (2005). Akt-dependent transformation: there is more to growth than just surviving. Oncogene *24*, 7435–7442.

Pullen, N., Dennis, P.B., Andjelkovic, M., Dufner, A., Kozma, S.C., Hemmings, B.A., and Thomas, G. (1998). Phosphorylation and activation of p70s6k by PDK1. Science *279*, 707–710.

Ranger, A.M., Zha, J., Harada, H., Datta, S.R., Danial, N.N., Gilmore, A.P., Kutok, J.L., Le Beau, M.M., Greenberg, M.E., and Korsmeyer, S.J. (2003). Bad-deficient mice develop diffuse large B cell lymphoma. Proc. Natl. Acad. Sci. USA *100*, 9324–9329.

Sabatini, D.M. (2006). mTOR and cancer: insights into a complex relationship. Nat. Rev. Cancer *6*, 729–734.

Siegers, K., Waldmann, T., Leroux, M.R., Grein, K., Shevchenko, A., Schiebel, E., and Hartl, F.U. (1999). Compartmentation of protein folding in vivo: sequestration of non-native polypeptide by the chaperonin-GimC system. EMBO J. *18*, 75–84.

Siegert, R., Leroux, M.R., Scheufler, C., Hartl, F.U., and Moarefi, I. (2000). Structure of the molecular chaperone prefoldin: unique interaction of multiple coiled coil tentacles with unfolded proteins. Cell *103*, 621–632.

Vainberg, I.E., Lewis, S.A., Rommelaere, H., Ampe, C., Vandekerckhove, J., Klein, H.L., and Cowan, N.J. (1998). Prefoldin, a chaperone that delivers unfolded proteins to cytosolic chaperonin. Cell *93*, 863–873.

Wu, X., Reiter, C.E., Antonetti, D.A., Kimball, S.R., Jefferson, L.S., and Gardner, T.W. (2004). Insulin promotes rat retinal neuronal cell survival in a p70S6K-dependent manner. J. Biol. Chem. *279*, 9167–9175.

Wullschleger, S., Loewith, R., and Hall, M.N. (2006). TOR signaling in growth and metabolism. Cell *124*, 471–484.

Yart, A., Gstaiger, M., Wirbelauer, C., Pecnik, M., Anastasiou, D., Hess, D., and Krek, W. (2005). The HRPT2 tumor suppressor gene product parafibromin associates with human PAF1 and RNA polymerase II. Mol. Cell. Biol. *25*, 5052–5060.